

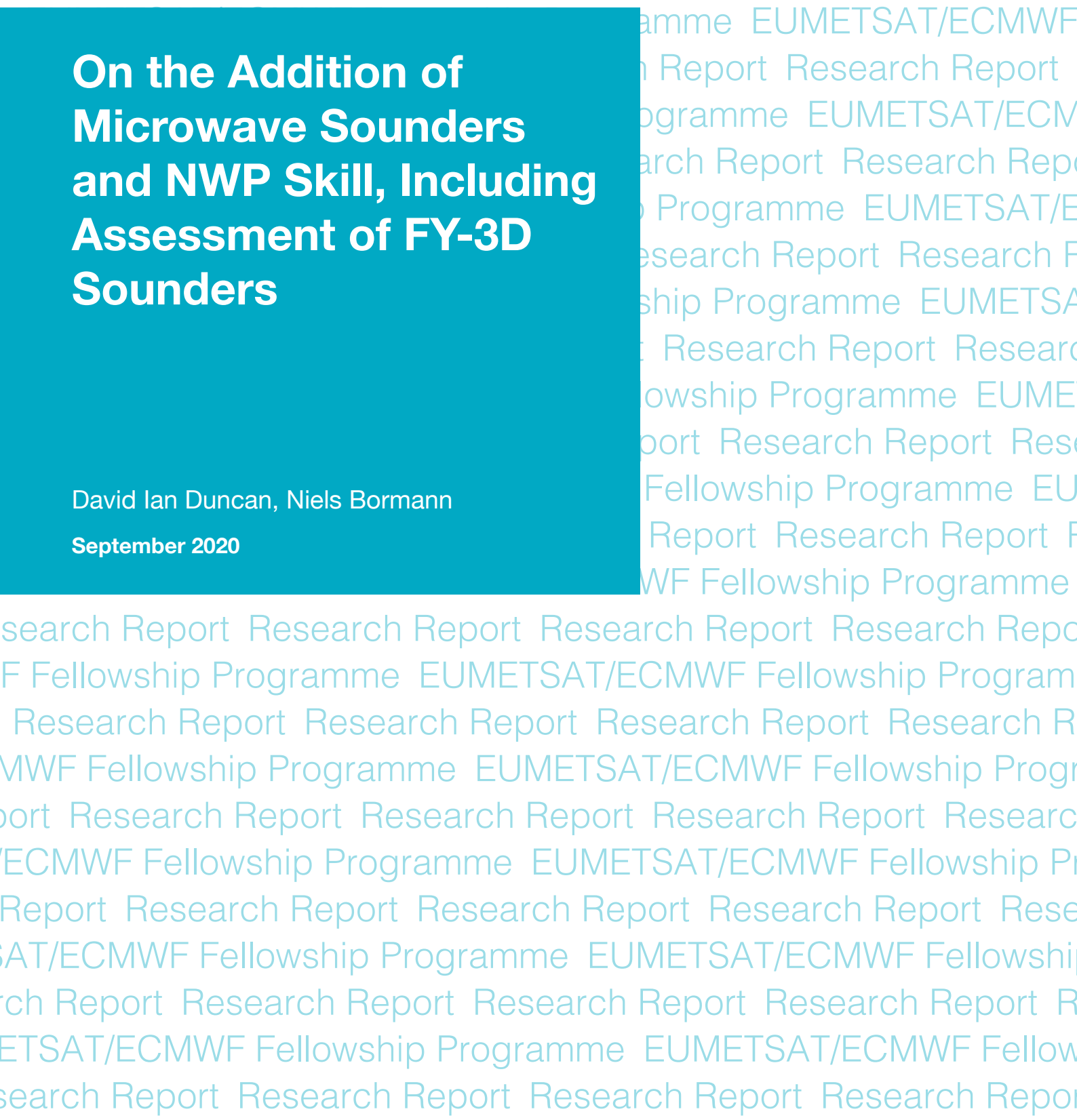
# EUMETSAT/ECMWF Fellowship Programme Research Report

# 55

## **On the Addition of Microwave Sounders and NWP Skill, Including Assessment of FY-3D Sounders**

David Ian Duncan, Niels Bormann

September 2020



Series: EUMETSAT/ECMWF Fellowship Programme Research Reports

A full list of ECMWF Publications can be found on our website under:

<http://www.ecmwf.int/en/research/publications>

Contact: [library@ecmwf.int](mailto:library@ecmwf.int)

© Copyright 2020

European Centre for Medium-Range Weather Forecasts, Shinfield Park, Reading, RG2 9AX, UK

Literary and scientific copyrights belong to ECMWF and are reserved in all countries. This publication is not to be reprinted or translated in whole or in part without the written permission of the Director-General. Appropriate non-commercial use will normally be granted under the condition that reference is made to ECMWF.

The information within this publication is given in good faith and considered to be true, but ECMWF accepts no liability for error or omission or for loss or damage arising from its use.

## Abstract

The utility of microwave sounding for numerical weather prediction (NWP) has been well established over many years, with these instruments comprising a reliable and indispensable part of the global observing system. But the volume of sounder data assimilated in NWP systems may change substantially in upcoming years, as there is an ageing constellation of satellites but also the prospect of proliferating small satellite constellations. This study examines the addition of temperature and humidity sounders from a baseline that includes no microwave sounders at all, aiming to elucidate the incremental benefit gained from adding sounders to the assimilation system. Framed as a series of observing system experiments (OSEs), large improvements in forecast skill and background fits to independent observations are gained from the addition of the first sounder. Significant further benefit is observed from additional sounders, with no saturation apparent in the maximal setup.

In the study's second part, the conclusion regarding lack of saturation from sounders is tested in the full observing system with the most recently activated microwave sounder at ECMWF, the humidity sounder on FY-3D. First, an assessment of data quality is given for both microwave sounders on FY-3D, MWTS-2 and MWHS-2, followed by analysis of forecast impact from the humidity sounder in research experiments prior to its activation in operations, which began December 2019. The success of adding FY-3D MWHS-2 to the current suite of microwave sounders shows that additional sounder observations still translate into improved forecasts, a finding that reinforces the conclusions of the paper's first half.

# 1 Introduction

## 1.1 Evolution of microwave sounding

Measurement of the natural emission of microwave (MW) radiation has been recognised as a priority of Earth observation for a long time (Njoku, 1982). From the perspective of atmospheric science and satellite meteorology more specifically, the “satellite era” began technically in the early 1960's with visible and infrared sensors, but accelerated in earnest with the Microwave Sounding Unit (MSU) instruments launched first in the late 1970's. These sensors exploited the oxygen absorption band between 50 to 60 GHz to provide global coverage of atmospheric temperature measurements of the troposphere and stratosphere. They possessed profiling capability despite having only four channels, and the technical challenge of retrieving reasonable temperature profiles from these measurements spurred the growth of variational (i.e. optimal estimation) techniques (Rodgers, 1976) that still underpin the mathematics of data assimilation systems today. The profiling capability of such sensors caused them to be called “sounders,” differentiated from microwave “imagers” that operate in atmospheric windows with less molecular absorption and thus have more sensitivity to the Earth's surface.

Sounding data from these early temperature sounding units was found useful in variational data assimilation for NWP (Andersson *et al.*, 1994) and also later in reanalyses, first as retrievals and then by direct radiance assimilation. Moving from the TOVS (Television and infrared observation satellite (TIROS) Operational Vertical Sounder) to the advanced TOVS (or ATOVS) observing platforms, the Advanced Microwave Sounding Unit-A (AMSU-A) has been in continuous operational use since the late 1990's and may be considered part of the backbone of the global observing system (English *et al.*, 2013). In mid 2020, seven AMSU-A sensors are actively assimilated at ECMWF, the most of any radiometer. The follow-on from AMSU-A is the Advanced Technology Microwave Sounder (ATMS), first launched on the Suomi National Polar-orbiting Partnership (SNPP) satellite in 2012, which combined most of the same temperature sounding channels from AMSU-A with five humidity sounding channels as well.

Three more ATMS sensors have yet to launch, so it is expected to remain a key part of the observing system for decades to come.

Humidity-sensitive channels from MW sounders did not see the same initial success in NWP as temperature sounders. Sampling around the strong water vapour absorption line at 183.31 GHz, these higher frequency observations are more sensitive to contamination from clouds and precipitation. But as assimilation techniques, radiative transfer codes, and the representation of clouds in models increased in sophistication, the additional sensitivity of humidity sounding channels has been recognised as a distinct advantage (Geer *et al.*, 2014). Whereas there were no MW humidity channels in the TOVS series, ATOVS featured channels for humidity sounding on the AMSU-B sensor. The SSMIS and SSM/T2 (Special Sensor Microwave Imager Sounder and Humidity, respectively) sensors also carried a suite of channels around 183 GHz. The successor to AMSU-B, the Microwave Humidity Sounder (MHS), is currently operational on five satellite platforms. Greater utilisation of humidity sounding channels is now recognised as a key reason behind NWP skill increases in recent years (Geer *et al.*, 2017).

Small satellite constellations could potentially transform the global observing system and provide greater spatiotemporal coverage of MW sounding measurements to better constrain atmospheric analyses of temperature and humidity (Blackwell *et al.*, 2018). However, the current observing system relies heavily on ageing sensors such as AMSU-A; for example, of the 7 AMSU-A sensors operationally assimilated at ECMWF in 2020, three are 15 years old or more (Aqua, NOAA-15, NOAA-18) and two more are over 10 years old (NOAA-19, Metop-A). In 2020 alone, capabilities have been lost or severely reduced on three actively assimilated humidity sounders (on FY-3B, FY-3C, Metop-A). Thus, while the future may bring significantly more sounding observations, it is also possible that total observation numbers will wane in intervening years as older sensors lose functionality before viable replacements are launched.

## 1.2 Observing System Experiments

A commonly used tool to assess the impact of a sensor or whole observation type in an NWP system is to conduct observing system experiments, or OSEs (Bouttier and Kelly, 2001). These are often framed as a data denial to implicitly determine the value of observations for NWP, to see the degradation of skill wrought by their absence and even assess synergies of observation types (Bormann *et al.*, 2019). More extreme OSEs may deny all satellite data (McNally *et al.*, 2014), while others may deny a single sensor to gauge its impact on the overall system.

This study takes advantage of a time period that may be considered part of a small golden age for MW sounding observations, as there were 8 different satellites with temperature sounding channels and 11 satellites with humidity sounding channels actively assimilated at ECMWF. While the sensors considered have differing channel complements and characteristics, this variety of platforms and its range of equator crossing times (ECT) provides an opportunity for a range of OSEs. Specifically, the range of sounders available is leveraged to assess their value when added incrementally to a global observing system without MW sounding data.

This study consists of two parts. In the first part, we conduct observing systems experiments with the presently available constellation of MW sounding data to systematically assess the benefits from incrementally adding the available orbits. This primarily characterises the impact from the currently existing constellation, but also provides a basis to gauge how much further impact might be expected from potential additional MW sounders in the future. In the second part, we investigate the latest addition of MW sounding data in the ECMWF system, that is, data from the humidity sounder on FY-3D. Both parts assess the benefits of incrementally adding additional MW sounders and hence provide important input

Table 1: Experiments summary table with experiment names and the satellites with sounding data active in the assimilation. For which sounders are actively used on each satellite, see Table 2.

Experiment Name	Satellites with Sounders Active
No Sounders	-
1 Sounder	NOAA-20
3 Sounders	NOAA-20, Metop-B, F-17, NOAA-15
5 Sounders	NOAA-20, Metop-B, F-17, NOAA-15, NOAA-18, NOAA-19
7 Sounders	NOAA-20, Metop-B, F-17, NOAA-15, NOAA-18, NOAA-19, SNPP, Metop-A

to the future evolution of the constellation of MW sounding data.

## 2 Sounders Addition

### 2.1 Data and Experimental Setup

The experiments described are all based on the ECMWF Integrated Forecast System (IFS) Cycle 46R1, run at TCo399 (approx. 25 km) L137 model resolution with 12-hour long window delayed cutoff assimilation cycles. The configuration is the same for all experiments—only the usage of the MW sounding data is changed. For all experiments, background errors are derived from the operational forecast system, or in other words represent a full observing system that includes all sounding data. While this is common practice for OSEs, as background error covariances are costly to recalculate, it is a limitation of the presented work and its effect is being investigated in a parallel study.

All experiments were run over the period June 1 to September 15, 2018, so 3.5 months in total. This period was chosen due to relatively few observing system changes occurring within it, and no significant channel failures on any of the sensors included. This period lies just after activation of NOAA-20 ATMS at ECMWF (May 2018) but before activation of Metop-C AMSU-A and MHS (March 2019) or FY-3D MWHS-2 (December 2019, see Section 3.3).

#### 2.1.1 Sounders Addition Experimental Setup

Table 1 gives a name to each experiment and which satellites' sounders were included in the assimilation. Our starting point is an experiment in which all MW sounding channels are removed from active assimilation, but otherwise the full observing system is used. We refer to this as the “No Sounders” experiment, and any channels in the 50 GHz or 118 GHz oxygen bands or the 183 GHz water vapour band from any instrument are excluded from active assimilation. This forms the baseline from which sounder data are added back into the assimilation system.

Following the No Sounders experiment, MW sounder data are added in stages, balancing relatively complementary orbits, and pairing temperature and humidity sensors together. Separate experiments were run with 1, 3, 5, and 7 MW temperature and humidity sounders added, as summarised in Tables 1 and 2. Mostly, we use ATMS or a combination of AMSU-A and MHS on the same satellite to form a

Table 2: Satellites with MW sounding sensors used in the study. The bottom of the table gives satellites with sounding channels used operationally at ECMWF during this time period but not assimilated in experiments within the study. Approximate local equator crossing times (ECT) for the descending node are given for the study period.

Satellite	T. Sensor	H. Sensor	ECT	Experiment(s)
<i>NOAA-20</i>	ATMS	ATMS	01:30	1, 3, 5, 7
<i>Metop-B</i>	AMSU-A	MHS	09:30	3, 5, 7
<i>DMSP F-17</i>	-	SSMIS	06:30	3, 5, 7
<i>NOAA-15</i>	AMSU-A	-	06:30	3, 5, 7
<i>NOAA-19</i>	AMSU-A	MHS	04:00	5, 7
<i>NOAA-18</i>	AMSU-A	MHS	08:00	5, 7
<i>SNPP</i>	ATMS	ATMS	01:30	7
<i>Metop-A</i>	AMSU-A	MHS	09:30	7
<i>Aqua</i>	AMSU-A	-	01:30	None
<i>DMSP F-18</i>	-	SSMIS	06:00	None
<i>FY-3B</i>	-	MWHS-1	03:30	None
<i>FY-3C</i>	-	MWHS-2	10:00	None
<i>GPM</i>	-	GMI	N/A	None

pair of temperature and humidity sounders. The exception is the third sounder which is a combination of AMSU-A on NOAA-15 and the 183 GHz channels of SSMI/S on DMSP-F17. These satellites have very similar early-morning equator crossing times during the period considered, and they are hence treated together here, as no early-morning satellite with both MW temperature and humidity sounding capabilities is presently available. Note that while ECTs are all different for the first 5 sounder pairs, the sixth and seventh sounders add instruments from satellites with an ECT similar to one already included.

The maximum number of MW sounders considered in the study is 7, representing the maximum number of available orbits for which both temperature and humidity sounding data are available. As can be seen in Table 2, there are further instruments with MW sounding channels, yet they provide only temperature or humidity sounding capabilities in a given orbit, but not a combination of both. The capabilities for some of these remaining instruments are more limited, due to fewer functioning channels or a more restricted usage.

### 2.1.2 Sounder Data

The channels employed as typical temperature and humidity sounding channels are given in Table 3. The temperature sounding sensors include only two, AMSU-A and ATMS, whereas the humidity sounding sensors include MHS, ATMS, and SSMIS. As the ATMS channel complement contains all sounder channels considered in this study, its channel numbers are a helpful reference when discussing the individual channels across the various sensors.

Some sensors like SSMIS and GMI have a mixed complement of channels. As the SSMIS temperature sounding channels are not actively assimilated at ECMWF, here we consider SSMIS and GMI to carry both imaging and humidity sounding channels. For SSMIS, only the 183 GHz channels' usage has been altered in these experiments; the imaging channels on SSMIS (F-17) were actively assimilated during this time, and they remain so. For GMI, in all experiments its 183 GHz channels were not assimilated while

Table 3: Actively assimilated channels on temperature and humidity sounding sensors, given by their bands' centre frequencies (C. Freq.) in GHz. As ATMS possesses all common channels, its channel numbers (ATMS Ch.) are given for reference.

Temperature			Humidity		
C. Freq.	ATMS Ch.	Other Sensors	C. Freq.	ATMS Ch.	Other Sensors
$53.596 \pm 0.115$	6	AMSU-A	$183.31 \pm 1.0$	22	MHS, SSMIS
54.40	7	AMSU-A	$183.31 \pm 1.8$	21	-
54.94	8	AMSU-A	$183.31 \pm 3.0$	20	MHS, SSMIS
55.50	9	AMSU-A	$183.31 \pm 4.5$	19	-
$57.290344 = f_0$	10	AMSU-A	$183.31 \pm 7.0$	18	MHS, SSMIS
$f_0 \pm 0.3222$	11	AMSU-A			
$f_0 \pm 0.3222 \pm 0.048$	12	AMSU-A			
$f_0 \pm 0.3222 \pm 0.022$	13	AMSU-A			
$f_0 \pm 0.3222 \pm 0.010$	14	AMSU-A			
$f_0 \pm 0.3222 \pm 0.0045$	15	AMSU-A			

all other channels were assimilated as in normal operations ([Lean et al., 2017](#)). Both SSMIS and GMI have channels in the 150 GHz to 166 GHz window region, and these are actively assimilated beginning with Cycle 46R1 ([Lonitz and Geer, 2020](#)). For our purposes here, these are considered imager channels despite their sensitivity to humidity via continuum absorption of water vapour, and thus remain active in all experiments.

Note that most sensors with sounding channels are cross-track instruments, in that they scan back and forth normal to the satellite's direction of motion and thus sound the atmosphere at various angles and levels. In contrast, one of the sensors we consider here, SSMIS, is conically scanning and thus views the atmosphere at a fixed angle off nadir in front of the satellite's direction of motion. SSMIS humidity channels are thus not exactly equivalent to MHS, for example, as the same frequencies are sensitive to humidity at different atmospheric levels due to the scanning strategy.

In these experiments, the treatment of data in the assimilation is unchanged from that in operations. AMSU-A and ATMS data are thinned as sensor groups together so as to manage the overall data volume and error correlations that may exist horizontally, and their data are assimilated in the clear-sky assimilation stream. The clear-sky assimilation stream includes no absorption or scattering from hydrometeors in the atmosphere, whereas the all-sky stream includes hydrometeors in the radiative transfer. 3x3 averaging of ATMS data is performed prior to assimilation to more closely match the noise performance of equivalent AMSU-A channels. For more details see [ECMWF \(2019a\)](#), [ECMWF \(2019b\)](#), [Geer et al. \(2014\)](#), and [Bormann et al. \(2013\)](#).

To help visualise the data usage, we can employ ATMS since it has all the temperature and humidity channels considered in these experiments. Channel numbers and centre frequencies for ATMS are found in Table 3, along with the sensors that have equivalent channels. A sample cycle is shown in Fig. 1, the 0Z assimilation window on September 1, 2018, indicating which channels were actively used and on which satellites. Seen from a different perspective, total observation numbers of ATMS channel equivalents are given in Fig. 2 for each experiment. Channel usage differs either because some instruments do not include all channels, or because certain channels have failed on certain instruments (especially for

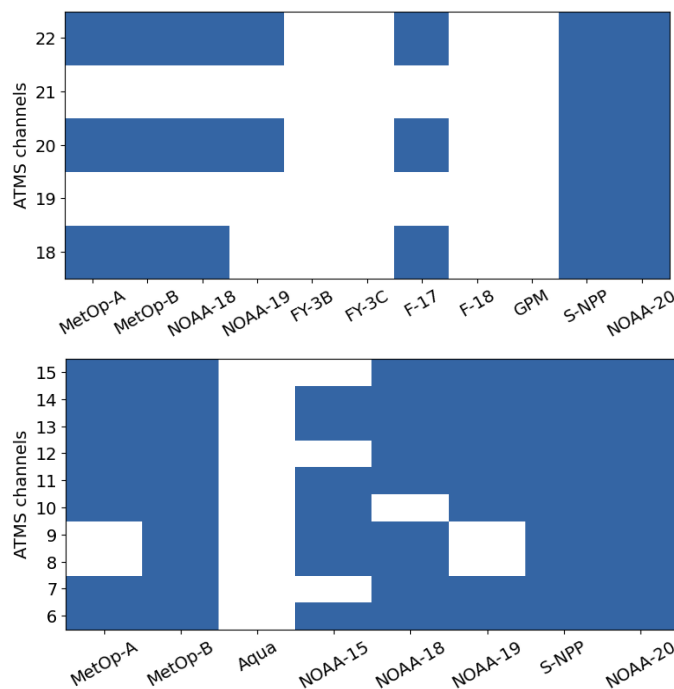


Figure 1: Data usage of assimilated sounding channels from the 7 Sounders experiment is shown in blue, indexed by ATMS channel numbers and separated into humidity (top) and temperature (bottom) channels, from a sample date (September 1, 2019) within the experimental period. Note how Aqua AMSU-A and humidity channels from FY-3B, FY-3C, F-18, and GPM are inactive due to satellite selection (see Table 2), whereas other channels either do not exist on some sensors or are broken and thus inactive.

AMSU-A and MHS). As apparent from Fig. 2, not every sounder pair added is equivalent, due to this different availability of channels, but also different clear-sky/all-sky usage in the assimilation. This needs to be kept in mind when comparing the impacts of different sounder increments.

## 2.2 Sounders Addition Results

Addition of MW sounding observations shows clear and strong beneficial impact on forecast scores well into the medium-range. From the depleted baseline with no MW sounding data, strong forecast improvement is visible in various fields. A consistent pattern emerges in which forecasts are very significantly improved at short lead times, 12 to 24 hours, and these benefits decrease at longer lead times but remain beneficial at the 95% confidence level. The strength of the forecast improvements and how long they last into the forecast period depend on the parameter and atmospheric level, but the general pattern is robust.

Forecast benefit is visible in root mean squared errors (RMSE) of 500 hPa geopotential heights (hereafter Z500) from introduction of the first sounder. Figure 3 shows that each further addition of sounder data (i.e. 3, 5, 7 sounders) yields a further reduction in Z500 RMSE, albeit to a somewhat smaller extent. The improvements are statistically significant out to 4-day lead times in both hemispheres for the 3, 5, and 7 Sounder experiments, for example. The overall impact of sounder data is stronger throughout the Southern Hemisphere (SH), where fewer conventional observations help to constrain the atmospheric analysis. This is clear when comparing the panels in both figures. For instance, the inclusion of 5 or 7 sounders demonstrates significant impact in SH Z500 out to forecast day 6 and 7, respectively (not

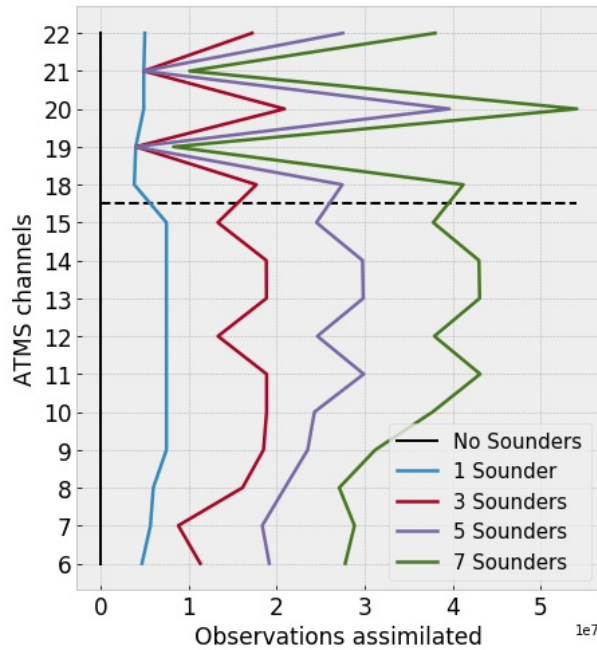


Figure 2: Total number of actively assimilated observations from sounding channels in each experiment, indexed by ATMS channel numbers and summed over the 3.5 month experimental period. The dashed line separates temperature sounding channels (6-15) from humidity sounding channels (18-22).

shown).

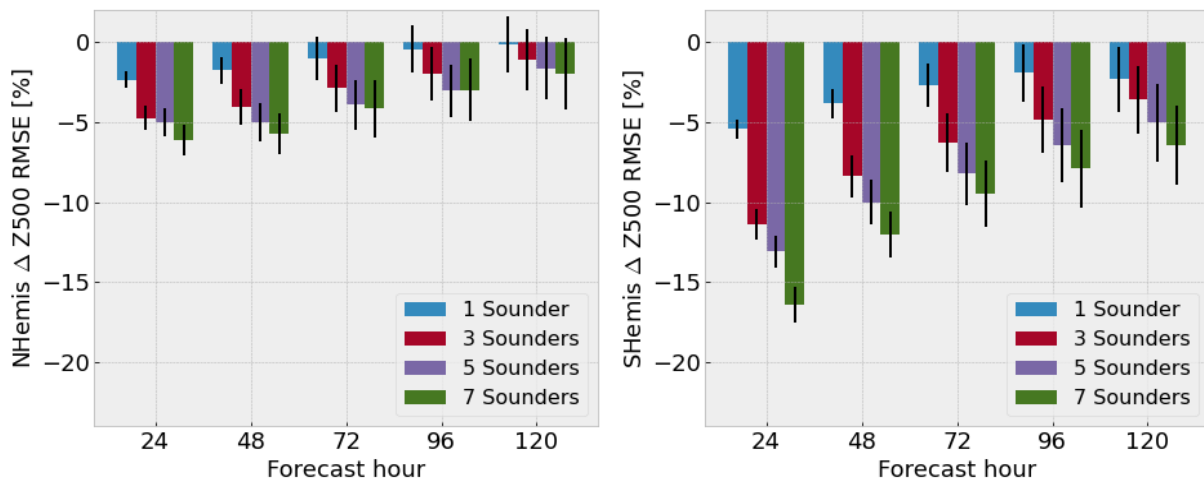


Figure 3: Change in geopotential height root mean squared errors (RMSE) at 500 hPa, given as a percent difference relative to No Sounders as the control. Forecast lead times are given on the x-axis in hours. The left panel shows scores over the Northern Hemisphere (20 °N to 90 °N) and the right panel shows Southern Hemisphere scores (20 °S to 90 °S). Two-tailed 95% confidence intervals are shown by black lines (following Geer (2016)), and the verification reference was the ECMWF operational analysis.

In the polar regions shown in Fig. 4, the benefit of adding at least one MW sounder pair is very clear in the Z500 scores, and further additions show strong additional benefits, indicating no apparent “saturation” for improving mid troposphere forecasts. This finding is in line with the significance of MW radiance

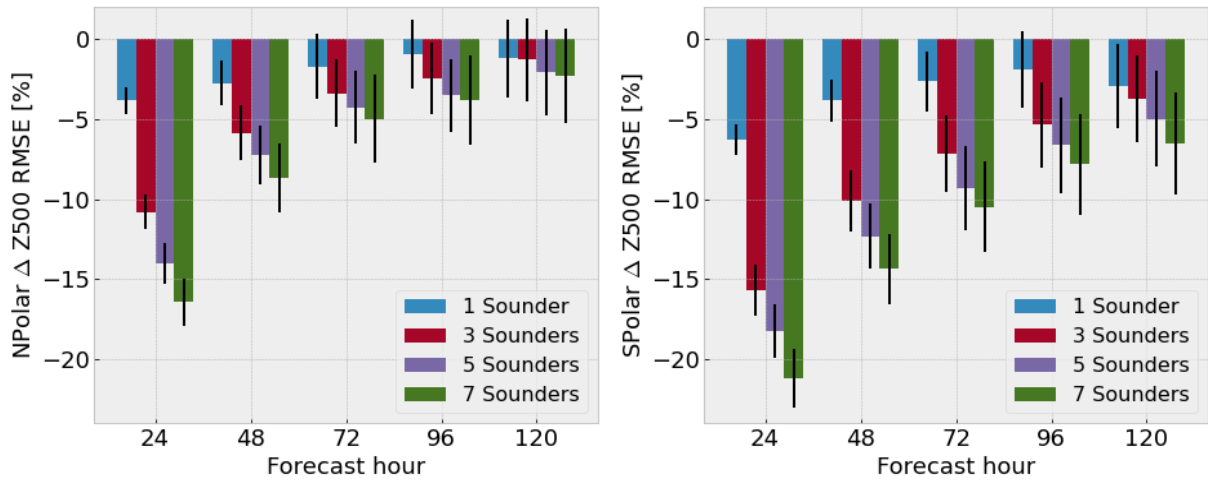


Figure 4: As in Fig. 3, but instead scores over the Arctic region (> 60 °N) on the left and the Antarctic region (> 60 °S) on the right.

assimilation in the Arctic noted elsewhere (Lawrence *et al.*, 2019). The large polar impacts seen here in both hemispheres are particularly noteworthy, as the poles are the most heavily-sampled regions on Earth due to most satellites maintaining polar orbits. The fact that improvements in Z500 scores are not only visible in the polar regions but actually strongest there with additional MW sounders is perhaps the strongest argument against saturation, given the high density of satellite observations there already.

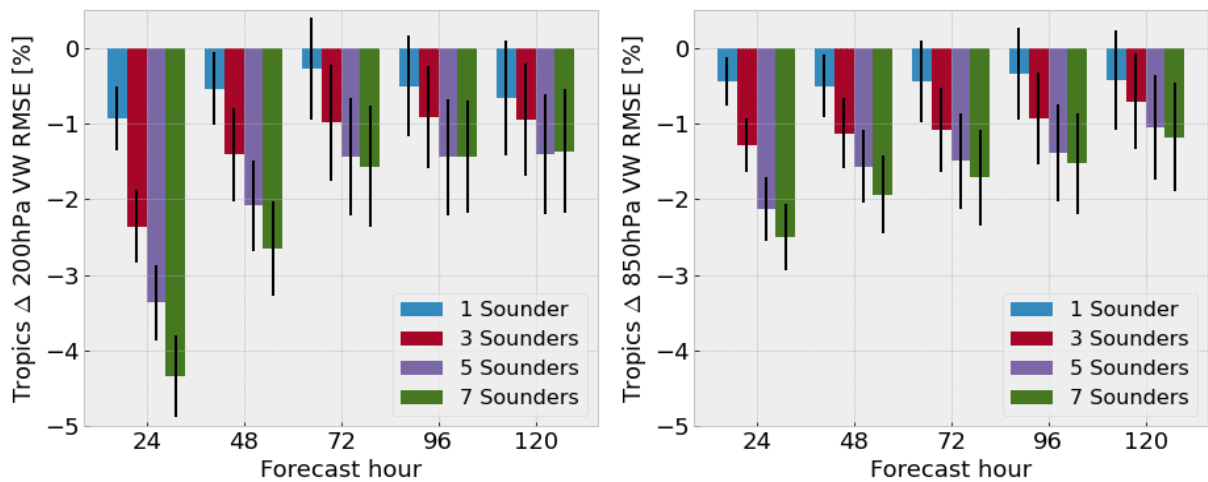


Figure 5: As in previous figures, but for vector wind (VW) RMSE over the tropical belt (20 °N to 20 °S), for 200 hPa (left) and 850 hPa (right).

Continued benefits from adding MW sounders are also seen in the Tropics. Figure 5 shows the change in RMSE for vector winds (VW) at 850 hPa and 200 hPa in the Tropics. The impact of sounder data is shown to be larger in the upper troposphere than the lower atmosphere. Some of this is likely through the “tracer effect,” by which 4D-Var derives wind information from the all-sky assimilation of humidity-sensitive observations (Geer *et al.*, 2017). At both levels in the Tropics, adding sounder data shows clear benefit well into the medium range.

Evaluation of short-range forecast scores against analyses can be misleading (Bormann *et al.*, 2019),

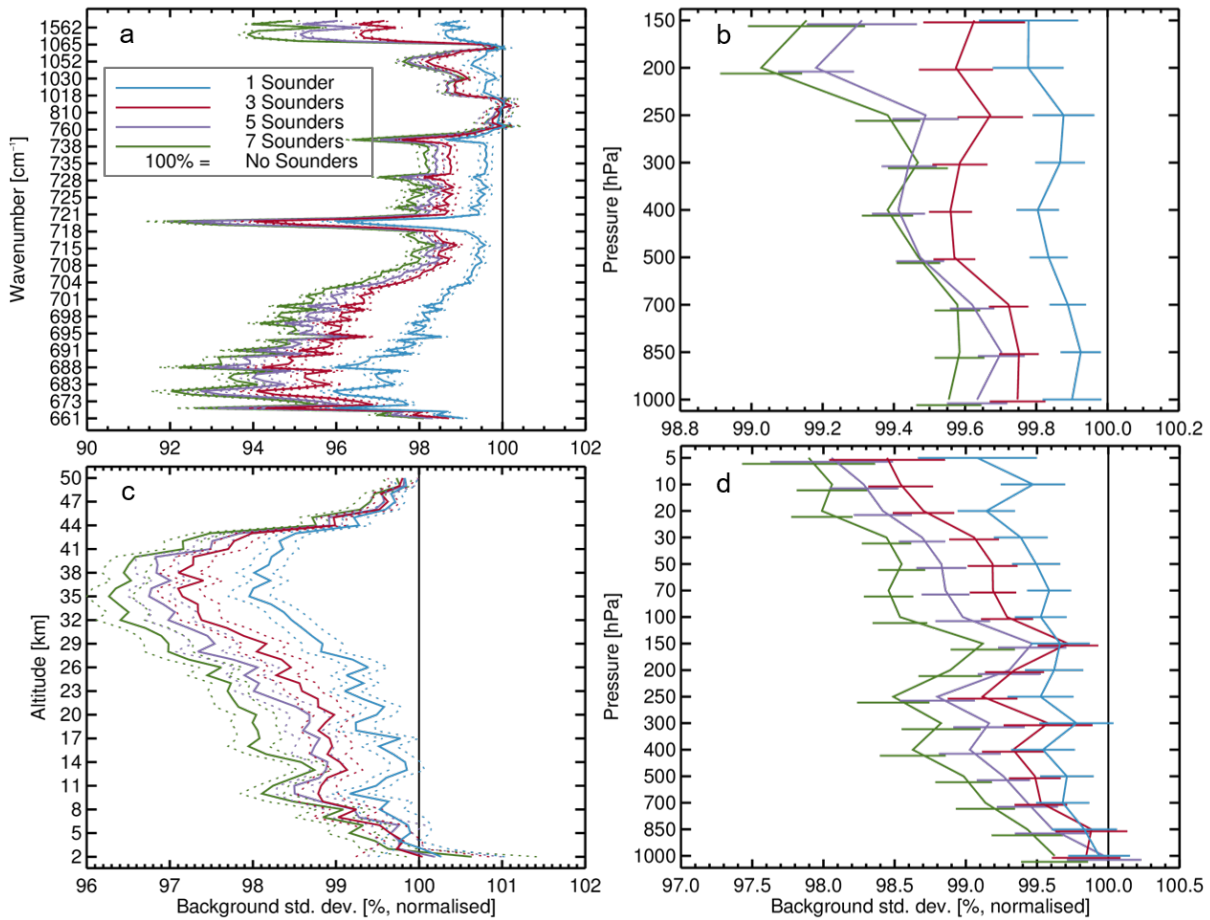


Figure 6: Changes in the global standard deviation of background departures for independent observations from adding sounder pairs. The percentage change in standard deviation of first guess (FG) departures is given for channels/levels from (a) CrIS, (b) AMVs, (c) GPS-RO, (d) radiosonde temperature. The 100% line indicates the No Sounders baseline. 95% confidence intervals are shown by horizontal lines (b, d) and dotted lines (a, c).

so in the following we further assess the short-range impact through background statistics for other assimilated observations. Fig. 6 shows global statistics for several observations with a strong signal in the O-B (observed minus background) fields. For each observation type, strong impact is seen from the first sounder added, as much as 1-2% decrease in the standard deviation for some background departures. The maximal 7 Sounders experiment yields a 3% or more decrease in the standard deviation of O-B for some observations—a remarkable amount considering that the rest of the observing system remains unchanged.

Analysing the short-range forecast fits against other observations gives a clear indication of where sounder data improves the analysis. Radio occultation (GPS-RO) fits are most improved in the mid stratosphere (about 25 to 40 km), where MW temperature channels are a vital constraint. The radiosonde fits also improve most at high altitudes, but there is a secondary peak below the tropopause that also appears in the atmospheric motion vector (AMV) fits. From the hyperspectral infrared sensor CrIS, its upper tropospheric and stratospheric channels (wavenumbers below about 700 cm<sup>-1</sup>) show the largest impact from MW sounder data being added, but the humidity channels (wavenumbers around 1050 cm<sup>-1</sup>) also show sizable impact that is quite distinct even between 5 and 7 Sounders. This view indicates a lack

of saturation for short-range forecasts at various atmospheric levels. These findings echo other recent studies (Bormann *et al.*, 2019; Weston and Bormann, 2018).

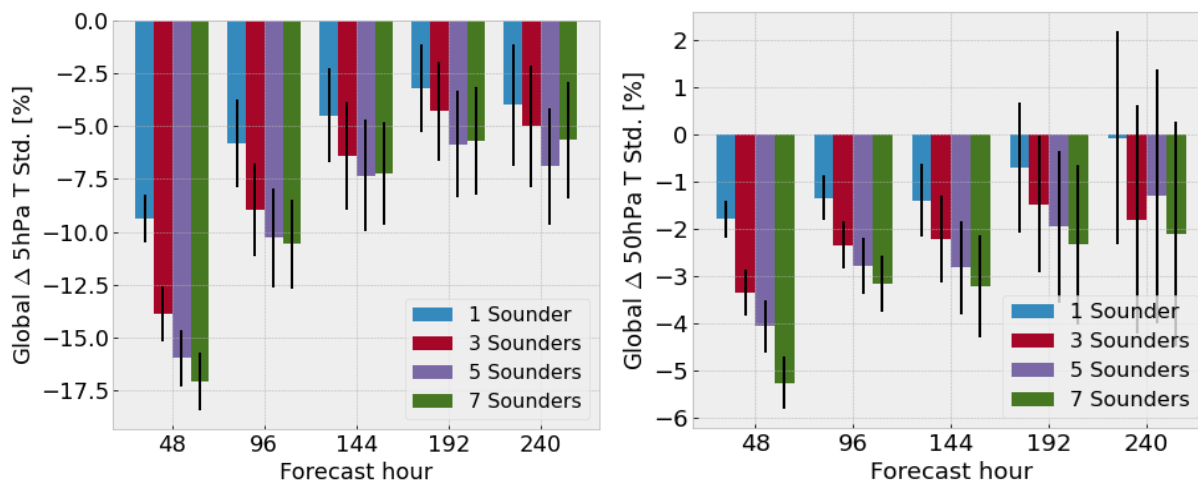


Figure 7: As in Fig. 3, but for global stratospheric temperature (T) error standard deviation, for 5 hPa (left) and 50 hPa (right). Note the different x-axis, spanning 2- to 10-day forecast lead times.

As hinted at in the short-range forecasts assessed in Fig. 6, the impact of MW sounder data may be largest in the stratosphere. Figure 7 shows the reduction of forecast error at two stratospheric pressure levels, 5 hPa and 50 hPa. Here we focus on temperature standard deviations (stratospheric biases can depend heavily on the verification reference) and look at longer lead times due to the slower processes involved. The impact of MW sounders in the stratosphere is relatively consistent with tropospheric impacts, with strong positive effects realised by the first sounder addition and further improvements from additional sounders lasting well into the medium range. Impacts are quantitatively largest in the upper stratosphere, as AMSU-A and ATMS act as key constraints on the analysis at these pressure levels. While significant impact is visible out to day 10 in the upper stratosphere, the apparent benefit of additional sounders gradually decreases at longer lead times.

### 3 FY-3D Sounding Instruments

In this second part of the paper, the focus shifts to a recent addition to the global observing system, FY-3D. The FY-3D satellite is the second member of the FY-3 series from CMA that is designated for operational use, following FY-3C and holding many of the same instruments. FY-3D was launched in November 2017 into a 14:00 ECT, with a real-time data stream established at ECMWF in summer 2019. Note that FY-3D is not included in earlier tables and figures for the sounder addition experiment (Table 2, Fig. 1) because the data were not available operationally over that time period.

First, the data quality of the two microwave sounding instruments on board FY-3D, MWHS-2 and MWTS-2 (Micro-Wave Humidity/Temperature Sounder -2, respectively), are assessed relative to similar sensors. Then, results of assimilation experiments using MWHS-2 are presented in the context of the paper's first half. For analysis of the FY-3 series considered altogether and its impact on forecast skill at ECMWF, including some assessment of the microwave imager on FY-3D, see Bormann *et al.* (in review).

MWTS-2 is a temperature sounder using a channel suite similar to AMSU-A, with 13 channels primar-

Table 4: Channels numbers (Ch.) and their central frequencies (C. Freq.) are given for MWTS-2 and MWHS-2, focusing on the actively assimilated channels only. Equivalent ATMS channel numbers are given if one exists, as in Table 3, with an asterisk signifying an inexact channel match.

MWTS-2			MWHS-2		
Ch.	C. Freq.	ATMS Ch.	Ch.	C. Freq.	ATMS Ch.
4	53.596	6*	2	$118.75 \pm .08$	-
5	54.40	7	3	$118.75 \pm 0.2$	-
6	54.94	8	4	$118.75 \pm 0.3$	-
7	55.50	9	5	$118.75 \pm 0.8$	-
8	$57.290 = f_0$	10	6	$118.75 \pm 1.1$	-
9	$f_0 \pm 0.217$	11*	7	$118.75 \pm 2.5$	-
10	$f_0 \pm 0.3222 \pm 0.048$	12	8	$118.75 \pm 3.0$	-
11	$f_0 \pm 0.3222 \pm 0.022$	13	11	$183.31 \pm 1.0$	22
12	$f_0 \pm 0.3222 \pm 0.010$	14	12	$183.31 \pm 1.8$	21
13	$f_0 \pm 0.3222 \pm 0.0045$	15	13	$183.31 \pm 3.0$	20
			14	$183.31 \pm 4.5$	19
			15	$183.31 \pm 7.0$	18

ily sampling the oxygen absorption band near 50 GHz, albeit without the window channels at 23.8 and 31.4 GHz. MWHS-2 holds five channels sampling around the strong water vapour absorption line at 183.31 GHz, just like on ATMS. What sets MWHS-2 apart amongst current operational sensors is its suite of channels sampling the weaker oxygen absorption line at 118.75 GHz. The channels of MWTS-2 and MWHS-2 are given in Table 4, alongside equivalent ATMS sounding channels. Both are cross-track scanning sensors. FY-3D has a nominal operating altitude of 836 km with a descending node local ECT of 02:00.

### 3.1 Data Quality Assessment

The payload of FY-3D includes three passive MW sensors as well as other instruments. Both of the MW sounder instruments are also present on board its predecessor, FY-3C. The MWHS-2 on board FY-3C was found to provide good quality observations, and thus most of its sounding channels have been assimilated operationally at ECMWF since 2016 (Lawrence *et al.*, 2018). FY-3C MWHS-2 is assimilated in the all-sky system, allowing scattering and absorption signals from hydrometeors to influence the assimilation. In contrast, FY-3C MWTS-2 exhibited striping, W-shaped scan biases, and orbital bias characteristics at various channels (Lu *et al.*, 2015), and is presently not assimilated in the ECMWF system. MWTS-2 is simulated via clear-sky radiative transfer, in line with the usage of AMSU-A and ATMS at ECMWF.

To assess the data quality of MWTS-2 and MWHS-2, background departures were examined first. These statistics can then be compared against equivalent channels on similar sensors. For MWTS-2, it is important to consider how the data are averaged when comparing to other sounders (Lu *et al.*, 2015); for MWTS-2, for now, we consider observations before and after 3x3 averaging. The 3x3 averaging is similar to what is done for ATMS (Bormann *et al.*, 2013), averaging out some of the instrument noise

to increase the signal to noise ratio. Note that the MWTS-2 scan pattern differs somewhat from that of ATMS, such that the effective footprints of MWTS-2 after 3x3 averaging are more elongated in the along-track direction. In contrast, MWHS-2 data are not averaged, though this is a possible topic for future investigation especially for its temperature sounding channels.

### 3.1.1 MWTS-2

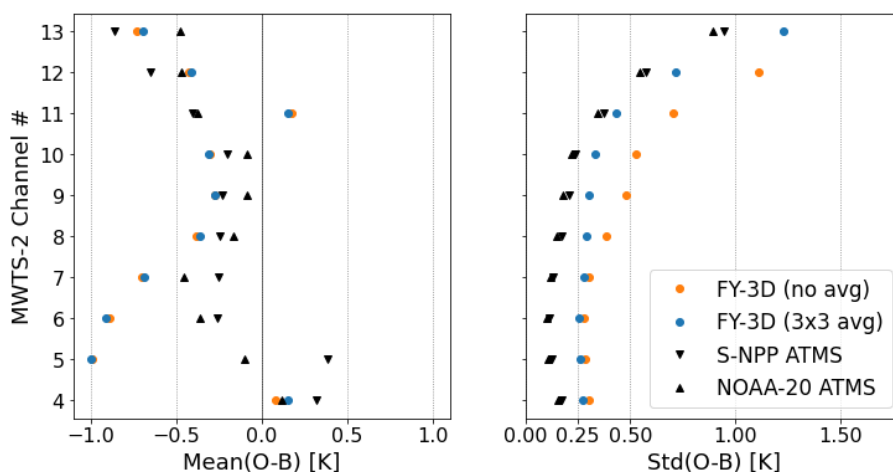


Figure 8: Background departure statistics for MWTS-2 over a sample week in mid July, 2019. Channels 1-3 have been omitted due to their surface sensitivity, and as they are used for screening rather than active assimilation. Mean O-B is shown in the left panel before bias correction (BC) is applied, and the right panel shows the standard deviation of O-B after BC. All data have been screened for cloud contamination, from observations over ocean. MWTS-2 data are given for un-averaged and 3x3 averaged observations, while ATMS data are for 3x3-averaged observations only.

Figure 8 shows background departure statistics for MWTS-2 for a sample week in July 2019. Most MWTS-2 channels exhibit a slight negative bias, but generally less than 1.0 K. The standard deviations of background departures show worse performance than equivalent ATMS channels on both NOAA-20 and SNPP; the use of 3x3-averaging improves std(O-B) significantly, especially for the stratospheric channels for which sensor noise is the dominant component of error, but the performance still lags behind that of ATMS. The small benefit of 3x3-averaging for the lower-peaking MWTS-2 channels, e.g. channels 4 to 7, would imply that random sensor noise is not the dominant cause of the poorer performance relative to ATMS. However, since MWTS-2 lacks the window channels on AMSU-A or ATMS typically used for cloud screening, the comparison is not perfect; the clear-sky criteria for MWTS-2 is set by a 3 K departure check on channel 1 alone, whereas for ATMS a cloud liquid water retrieval and scattering index inform the cloud proxy as well. For instance, it is possible that this clear-sky screening difference might manifest in the mean O-B for channel 4, which is about 1.0 K higher on FY-3D than for channels 5 or 6.

To examine the behaviour of background departures more closely, these can be analysed relative to scan position. While there is significant variation between channels and their scan bias structures, a sample is given here in Fig. 9 for channel 6. The scan position biases of this channel (top panel), are ultimately not handled well by the bias correction scheme, as the middle panel shows. This shape of scan bias, roughly W-shaped, is not represented well by the variational bias predictors used for temperature sounders, which include linear, quadratic, and cubic predictors for scan position bias. The residual scan position biases

after correction then map onto variability in the standard deviation of background departures, seen in the bottom panel. This seems to be a key factor in explaining the higher  $\text{std}(\text{O-B})$  relative to ATMS seen for this channel in Fig. 8.

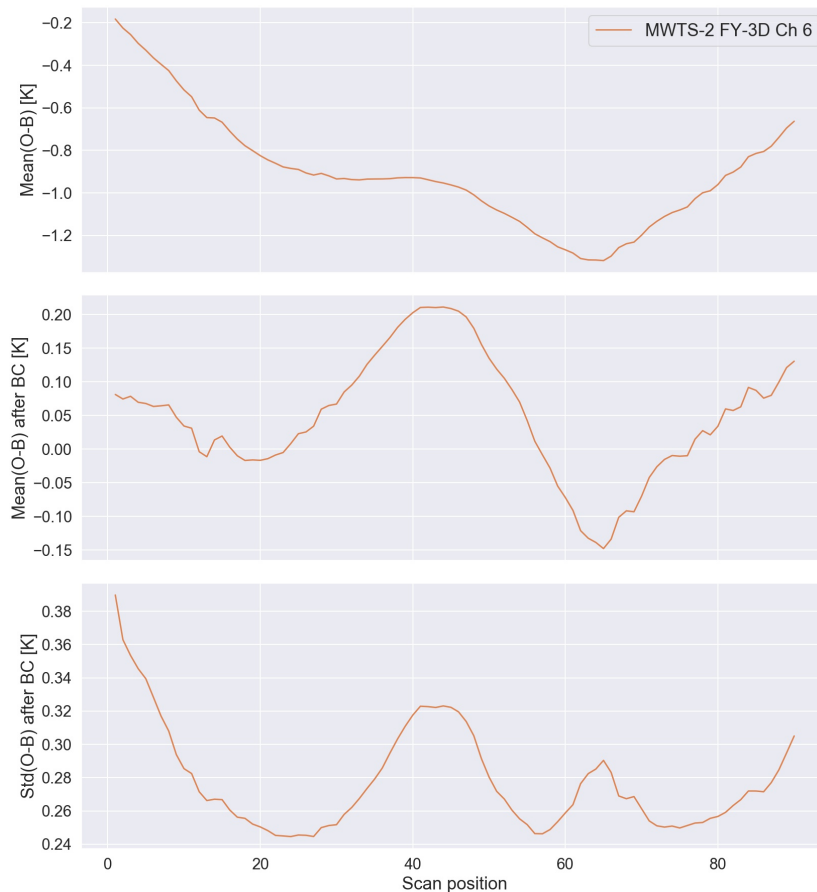


Figure 9: Background departure statistics given as a function of scan position for MWTS-2 channel 6 for a sample week in mid July, 2019. Panels show mean O-B before correction (top), mean O-B after bias correction (middle), and standard deviation of O-B after correction (bottom).

Lastly, a global map of background departures for a sample channel is given in Fig. 10, taken from operational monitoring on 4th July, 2020; the data are not screened, as can be seen by cloud and high orography signals in some places, but 3x3-averaging has been applied and the departures are shown after bias correction. The scan position biases for channel 5 mirror those of channel 6 in Fig. 9. Some occasional striping is also evident at this channel, but it is not pronounced. No orbital biases are noted for this channel, though a weak ascending/descending bias was seen for channel 13 (not shown).

In this short assessment, a comparison to FY-3C is not offered for MWTS-2 because the sensor on FY-3C was switched off in 2015 and therefore there is no period of overlap for direct comparison. However, some qualitative comparison is possible given the documentation from [Lu \*et al.\* \(2015\)](#). Channels 8 and 9 appear to perform substantially better for FY-3D than on FY-3C, which showed anomalously poor noise performance, whereas on FY-3D their  $\text{std}(\text{O-B})$  is in line with those of other channels. Also in that assessment, FY-3C exhibited strong negative biases of about 2-4K with respect to the background, compared to the much smaller negative biases seen here (Fig. 8). Despite these noted improvements, FY-3D exhibits some issues previously seen on FY-3C, including striping and scan position biases that

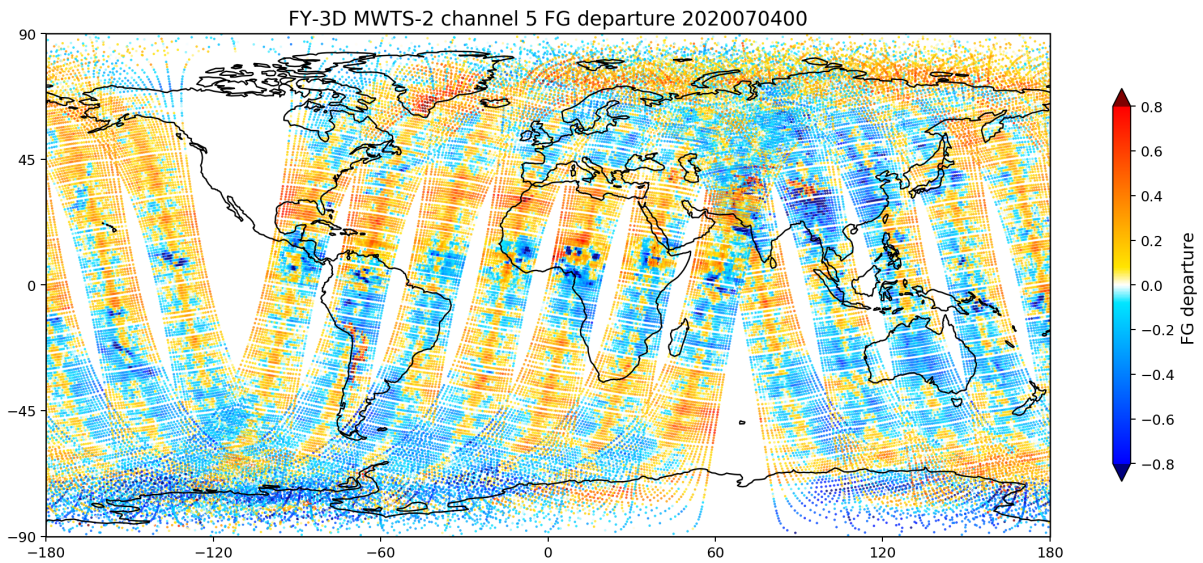


Figure 10: FY-3D MWTS-2 first guess departures (after bias correction) from operational monitoring, shown for channel 5 on July 4th, 2020.

are difficult to mitigate with the current bias correction scheme, as shown.

### 3.1.2 MWHS-2

The predecessor instruments to FY-3D MWHS-2 have seen success in the ECMWF system, with FY-3B MWHS-1 being actively assimilated from September 2014 through May 2020 when it was switched off, and FY-3C MWHS-2 used actively from April 2016 through the time of writing. This permits assessment of FY-3D to include direct comparison with its predecessor instrument on FY-3C.

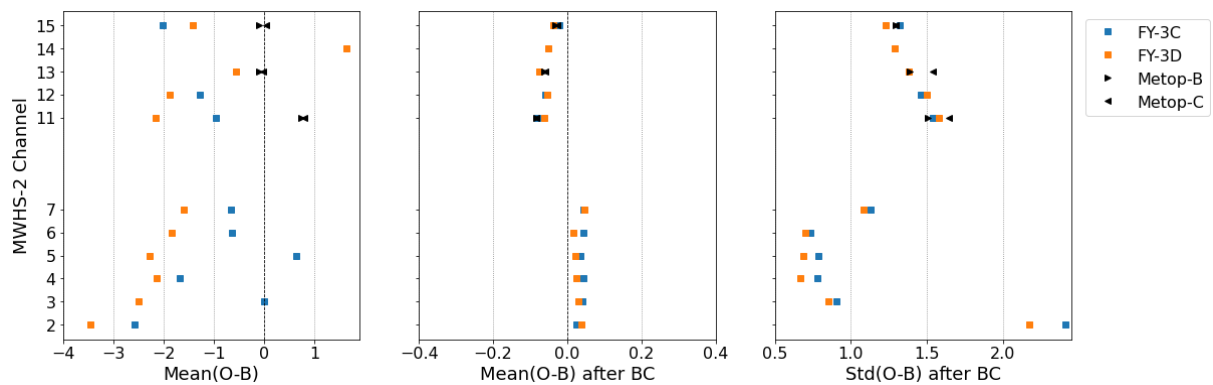


Figure 11: MWHS-2 background departure statistics from September 2019, from both FY-3C and FY-3D. Statistics from MHS on two platforms, Metop-B and Metop-C, are provided for comparison. The panels show background departure bias before correction (left), after bias correction (middle), and standard deviation of background departures after correction (right). Data were screened for used observations, over ocean, between 60 °N and 60 °S, and identified as relatively cloud-free using a scattering index check as in Lawrence *et al.* (2018).

Figure 11 compares background departure biases and standard deviations between FY-3C and FY-3D for

the MWHS-2 instrument. Statistics for equivalent channels on MHS from two satellites are provided for comparison. FY-3D exhibits large negative biases before correction, consistent with FY-3C but in fact more pronounced; however, after bias correction each channel has a mean bias near zero (middle panel). The bias characteristics of channels 13 and 14 on FY-3D are somewhat anomalous on the instrument, as all other channels exhibit similarly strong negative biases, but also are handled well by the correction scheme. Large changes in bias as well as orbitally-dependent biases have been noted previously for these channels on FY-3C (Lawrence *et al.*, 2018; Bormann *et al.*, in review), so this is something to keep an eye on. The improvements in background departure standard deviations at most channels are very promising, most markedly evident for channels 4 and 5. The NEDT for the 118 GHz channels on MWHS-2 are larger than other sources of error, so this improvement from FY-3C to FY-3D most likely reflects improved sensor noise for these channels on FY-3D.

The scan position biases should also be examined for MWHS-2, as strong asymmetric biases were noted previously for the first scan positions on FY-3C, and these were hence not assimilated at ECMWF (Lawrence *et al.*, 2018). Figure 12 shows scan position biases for a sample channel, comparing FY-3C and FY-3D. The scan position statistics given for channel 5 are fairly representative of the 118 GHz channels, capturing the main differences between FY-3C and FY-3D. Whereas strong scan position biases existed for FY-3C, these have mostly been improved for FY-3D and the overall fit to the background is improved across the scan. FY-3D generally exhibits larger absolute bias against the background but the bias correction handles this well. As seen clearly in the bottom panel, channel 5 on FY-3D shows a better fit to the background overall than on FY-3C. The humidity sounding channels on FY-3D mostly exhibit little in scan position biases after correction. Small asymmetric scan position biases were seen for channels 13 and 15 on FY-3D (not shown), and as a result the first scan positions are blacklisted for these two channels. The full scan width is used for all other FY-3D channels.

As noted by Lawrence *et al.* (2018), channels 13 and 14 on FY-3C were not actively assimilated for years due to concerns about their bias characteristics, and these channels also exhibited a weak but significant ascending/descending orbital bias that showed seasonal dependence (Bormann *et al.*, in review). These are therefore not present in Fig. 11, which displays used data from September 2019. These channels on FY-3D have not displayed such strong bias shifts or ascending/descending bias characteristics yet to date, and thus were not removed from active use in assimilation trials. These combined factors—more scan positions used and two more humidity channels actively used—mean that FY-3D has a higher data volume of used observations than FY-3C.

### 3.2 Assimilation Trials

Following the positive assessment of FY-3D MWHS-2, assimilation trials were run to ascertain the forecast impact of actively using these data. This was done using the standard TCo399 4D-Var experimental setup for assessing operational changes. The observing system in these experiments includes all satellite sensors used in operations as of May 2019. The assimilation experiment was run from mid July to mid November 2019, just over four months in total. The control and experiment are based on the IFS Cycle 46R1, which became operational in summer 2019.

The forecast impact of adding FY-3D MWHS-2 is neutral to slightly positive in the medium-range (Fig. 13). The largest improvements are seen for the Southern Hemisphere, where forecast errors for the 500 hPa geopotential are statistically significantly reduced by up to 1% in the day 2-4 range. There are also indications of forecast benefit over the South Pole, but not robustly significant given the four month period. A slight mean change in mid-tropospheric temperature in the Tropics leads to a small short-range degradation that disappears by day two, reminiscent of recent work on all-sky assimilation

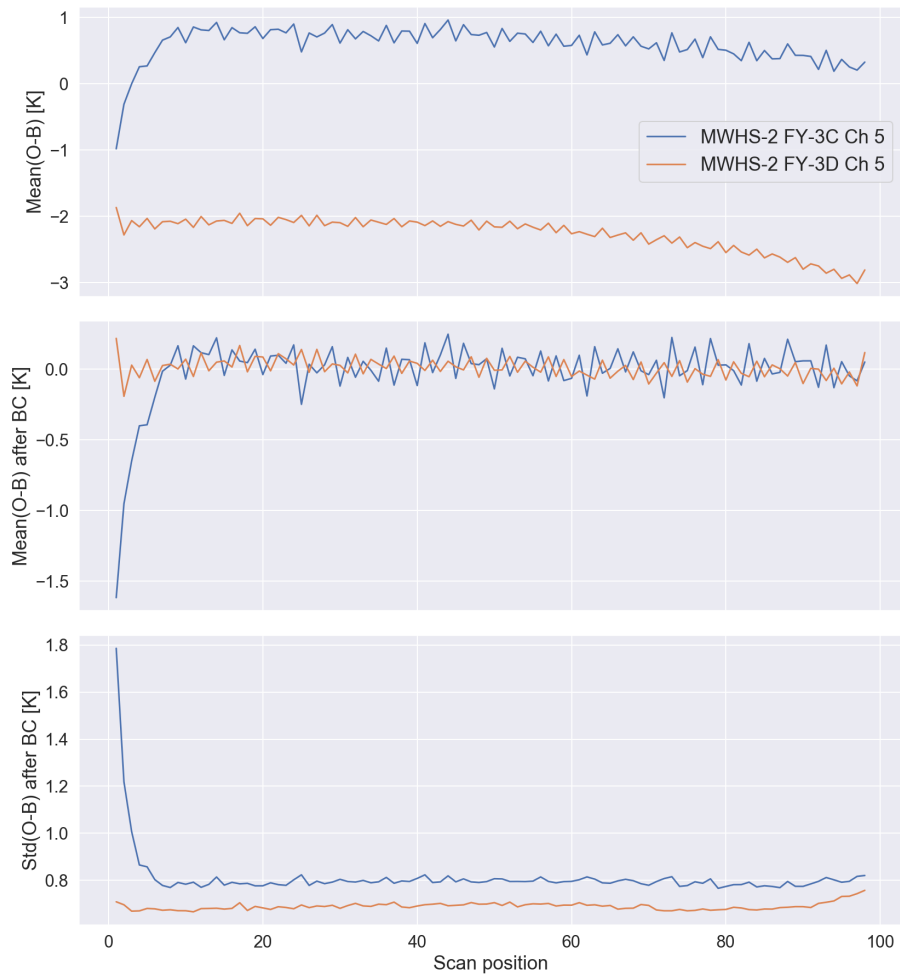


Figure 12: Channel 5 background departures as a function of scan position for MWHS-2 on FY-3C and FY-3D. Mean O-B before bias correction (top), after bias correction (middle), and standard deviation of O-B (bottom) are given for cloud-screened data over ocean from a sample week in July 2019.

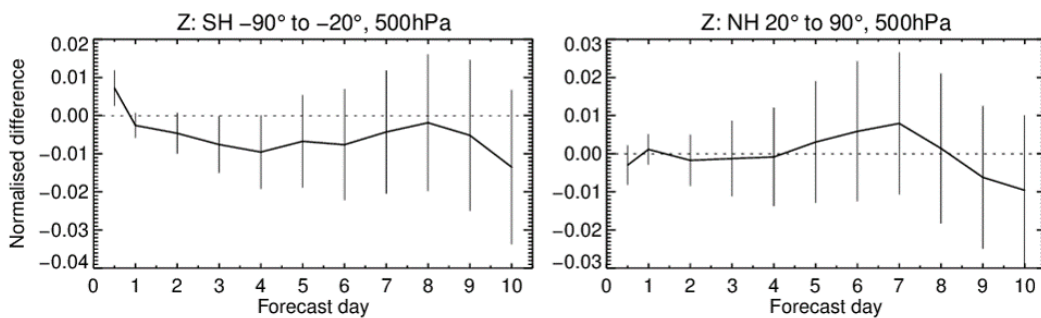


Figure 13: Root mean squared errors in Z500 scores are given for the Southern (left) and Northern (right) hemispheres. Verification is against own analysis, and the vertical lines represent confidence intervals of 95% given a two-tailed test.

of AMSU-A (Weston *et al.*, 2019). In the stratosphere, no forecast impacts show significance beyond a neutral result.

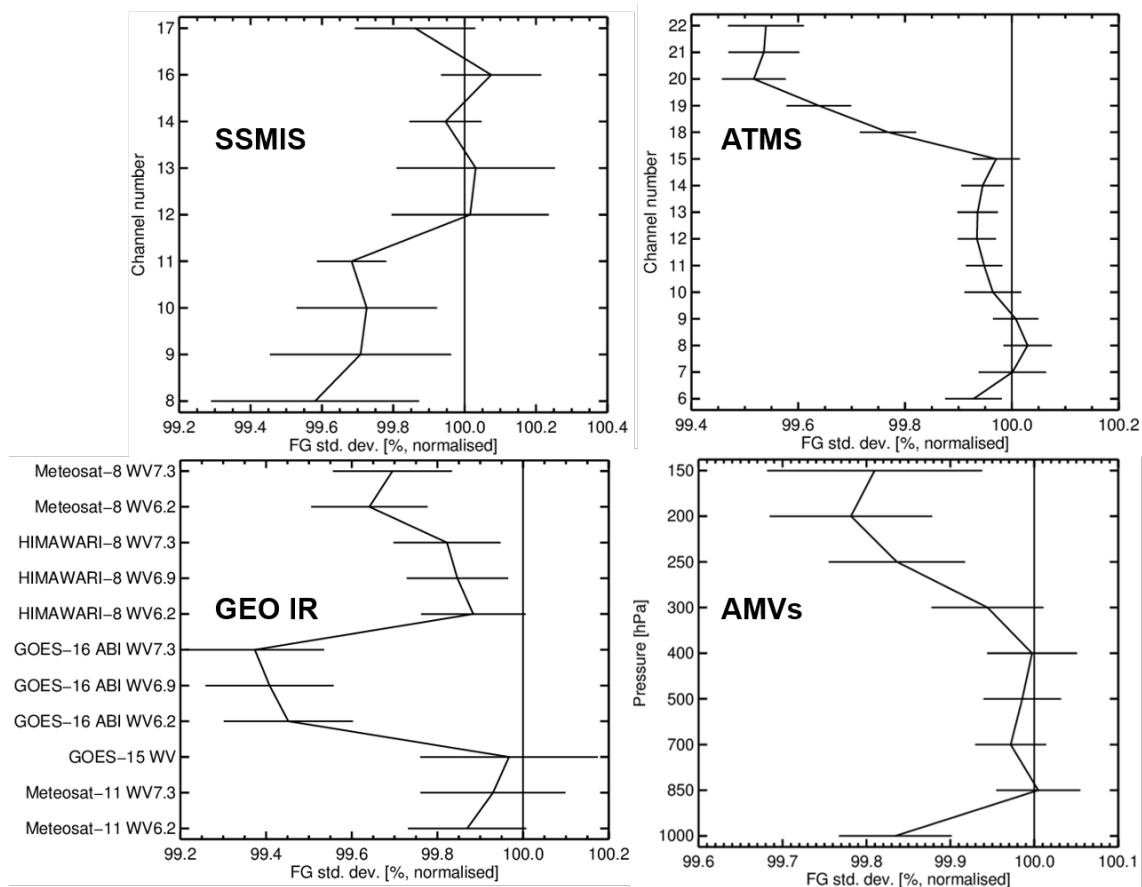


Figure 14: Change in the standard deviation of background departures, given as a percent difference relative to the control (100% line). The top panels are for SSMIS (left) and ATMS (right), the bottom panels show geostationary infrared water vapour channels (left) and atmospheric motion vectors (right).

To further evaluate the impact of the assimilation of MWS-2 on short-range forecasts, we also considered background departure fits for other assimilated observations. In general, the addition of FY-3D data improves background fits of most humidity-sensitive observations, from passive microwave to infrared. Figure 14 gives the changes in background fit for four other observing systems. ATMS background fits improve significantly for most active channels, but most especially for humidity sounding channels (18-22). The slight improvement for some stratospheric channels (11-14) was also observed in the assimilation of FY-3C MWS-2 (Lawrence *et al.*, 2018), where it was only present for the combined assimilation of the 118 GHz and 183 GHz channels. SSMIS sees improved fits for its 183 GHz channels (9-11) as well as channel 8 at 150 GHz, indicating the mutual benefit of increased humidity-sensitive MW channels used in all-sky assimilation, whereas the imager channels on SSMIS show no significant change. Geostationary infrared water vapour fits also witness significant improvement in most cases. Lastly, AMVs show improved fits in the upper troposphere and near the surface. Not shown in the figure, but also significant, is that the inclusion of FY-3D causes the number of AMV observations assimilated to increase by about 0.5% throughout the troposphere.

### 3.3 Discussion

The above assessment of FY-3D for its two MW sounding sensors led to MWHS-2 being activated in operations in December 2019, while MWTS-2 is currently being monitored. Later, the microwave imager on board FY-3D, MWRI, was found to have sufficient quality to be activated as a fourth imager in operations (Bormann *et al.*, *in review*), and this activation occurred in May 2020. Thus at the time of writing, FY-3D is a considerable component of the overall microwave constellation used in the ECMWF assimilation system. This is all the more relevant, as its predecessor sensors on FY-3B and FY-3C have been recently either switched off or are severely limited due to power issues.

MWHS-2 on FY-3D has become one of the dominant sources of data in the all-sky stream at ECMWF. Compiled statistics from January through mid June of 2020 indicate that nearly half a million FY-3D observations are assimilated in a mean 12 h assimilation cycle in operations, more than any other all-sky sensor and roughly the same as one ATMS. Furthermore, FY-3D MWHS-2 has a significant influence on the forecast as judged by the forecast sensitivity to observation impact (FSOI)—it averaged 2.3% of overall FSOI over the same period, similar in magnitude to F-17 SSMIS or an AMSU-A.

Following FY-3D, the next satellite in the FY-3 series is due to launch in 2021 into a relatively unique, early-morning orbit. FY-3E is expected to carry another MWHS-2 sensor and a new MW temperature sounder as well. Given the results presented here, the positive impact seen from assimilating the humidity sounder on FY-3D may be hoped to be repeated or even improved upon for FY-3E, given its unique orbital crossing time.

The results from assimilating MWHS-2 on FY-3D complement well the conclusions of the sounders addition study. Whilst the very large forecast improvements seen from the first sounders added (Fig. 3) are not replicated by the latest sounder, there is measurable impact that is neutral to positive (Figs. 13, 14). This lines up with theory and results from the sounder addition study, in that the impact of additional sounder observations may asymptote over time as sounders are added, but should remain positive if the information added is well characterised. It is possible, for instance, that spatially- or spectrally-correlated errors could confound this concept of adding information, but that does not seem to be the case here.

While the conclusions about humidity impacts from FY-3D MWHS-2 are relatively straightforward, conclusions regarding the utility of its 118 GHz channels are not. This echoes Lawrence *et al.* (2018), who found little direct impact from these channels when assessed on FY-3C alone. However, now with two MWHS-2 sensors in orbit with a good period of overlap, further study into optimising these channels' usage and assessing their combined impact may be warranted.

## 4 Conclusions

In this paper, the topic of additional microwave sounder data and its relative utility in NWP has been explored in two ways. One was a systematic and controlled assessment of the topic, feasible thanks to the large number of sounders currently in orbit so that sets of sensors could be added to a synthetically depleted observing system. The other was very practical, borne out of routine evaluation of a new data source to determine whether it was suitable for operational assimilation.

First, a series of OSEs were compared to a depleted observing system, with MW sounders added gradually in complementary pairs of temperature and humidity sensors from a variety of orbital crossing times. Improvements in forecast skill were dramatic for the first sounders, and remained consistently positive but gradually diminished up through the final sounders added. This was remarkably visible in almost ev-

ery metric examined, with positive impacts seen for parameters in all regions, throughout the troposphere and stratosphere, with only the magnitude of the response varying. Impacts were largest in the mid troposphere and upper stratosphere, especially in the Southern Hemisphere and polar regions where satellite data is predominant; the continued improvement in polar regions is particularly impressive, given that these regions already have high sampling from satellites.

Second, sounders from the FY-3D satellite were assessed relative to similar instruments. MWTS-2 showed some issues similar to its predecessor on FY-3C, with complex bias characteristics that are currently not handled well by the correction scheme in place. MWHS-2 performed similarly to currently used humidity sounders, and its temperature channels' performance is improved relative to FY-3C. The positive assessment of MWHS-2 led to trials that demonstrated the benefits of additional humidity sounding channels in assimilation, with improved humidity analysis and short-range forecasts as judged by other humidity-sensitive observations. Some mid-tropospheric forecast benefit was also visible into the medium range, demonstrating the potential of forecast benefit from further humidity sounders in particular.

These two studies taken together indicate that any type of “saturation” of MW sounder data in the ECMWF data assimilation system has not yet been reached. Adding sounders with well-characterised biases and low sensor noise to the observing system would be expected to add further to the quality of analyses and forecasts, as there is no strong indication in this work of such observations conflicting with any others. It is remarkable that a sensor like FY-3D MWHS-2 can provide demonstrable forecast benefits despite the plethora of similar channels already assimilated. But with some sounders breaking and many now far beyond their expected lifetime, this paper is a reminder not to take this abundance for granted either, as each one counts.

## Acknowledgements

David is supported by the EUMETSAT Fellowship Programme. Many thanks to Heather Lawrence and Peter Weston. Thanks as well to Stephen English for his helpful comments on the manuscript.

## References

- Andersson, E., Pailleux, J., Thépaut, J.-N., Eyre, J. R., McNally, A. P., Kelly, G. A. and Courtier, P. (1994). Use of cloud-cleared radiances in three/four-dimensional variational data assimilation. *Quart. J. Roy. Meteor. Soc.*, **120**(517), 627–653, doi:10.1002/qj.49712051707, URL <https://rmets.onlinelibrary.wiley.com/doi/abs/10.1002/qj.49712051707>.
- Blackwell, W. J., Braun, S., Bennartz, R., Velden, C., DeMaria, M., Atlas, R., Dunion, J., Marks, F., Rogers, R., Annane, B. and Leslie, R. V. (2018). An overview of the TROPICS NASA Earth venture mission. *Quart. J. Roy. Meteor. Soc.*, **144**(S1), 16–26, doi:10.1002/qj.3290, URL <https://rmets.onlinelibrary.wiley.com/doi/abs/10.1002/qj.3290>.
- Bormann, N., Duncan, D., English, S., Healy, S., Lonitz, K., Chen, K., Lawrence, H. and Lu, Q. (in review). Growing operational use of FY-3 data in the ECMWF system. *Adv. Atmos. Sci.*
- Bormann, N., Fouilloux, A. and Bell, W. (2013). Evaluation and assimilation of ATMS data in the ECMWF system. *J. Geophys. Res. Atmos.*, **118**(23), 12,970–12,980, doi:10.1002/2013JD020325, URL <https://agupubs.onlinelibrary.wiley.com/doi/abs/10.1002/2013JD020325>.
- Bormann, N., Lawrence, H. and Farnan, J. (2019). Global observing system experiments in the ECMWF assimilation system. *Technical Report 839*, ECMWF Tech. Memo., doi:10.21957/sr184iyz, URL <https://www.ecmwf.int/node/18859>.
- Bouttier, F. and Kelly, G. (2001). Observing-system experiments in the ECMWF 4D-Var data assimilation system. *Quart. J. Roy. Meteor. Soc.*, **127**(574), 1469–1488, doi:10.1002/qj.49712757419, URL <https://rmets.onlinelibrary.wiley.com/doi/abs/10.1002/qj.49712757419>.
- ECMWF (2019a). *IFS Documentation CY46R1, Part I: Observations*. ECMWF, URL <https://www.ecmwf.int/node/19305>.
- ECMWF (2019b). *IFS Documentation CY46R1, Part II: Data Assimilation*. ECMWF, URL <https://www.ecmwf.int/node/19306>.
- English, S., McNally, A., Bormann, N., Salonen, K., Matricardi, M., Horányi, A., Rennie, M., Janiskova, M., Michele, S. D., Geer, A. J., di Tomaso, E., Cardinali, C., de Rosnay, P., Sabater, J., Bonavita, M., Albergel, C., Engelen, R. and Thépaut, J.-N. (2013). Impact of satellite data. *Technical Report 711*, ECMWF Tech. Memo., doi:10.21957/b6596ot1s, URL <https://www.ecmwf.int/node/9301>.
- Geer, A., Baordo, F., Bormann, N., Chambon, P., English, S., Kazumori, M., Lawrence, H., Lean, P., Lonitz, K. and Lupu, C. (2017). The growing impact of satellite observations sensitive to humidity, cloud and precipitation. *Quart. J. Roy. Meteor. Soc.*, **143**(709), 3189–3206, doi:10.1002/qj.3172.
- Geer, A. J. (2016). Significance of changes in medium-range forecast scores. *Tellus A*, **68**(1), 30229, doi:10.3402/tellusa.v68.30229.
- Geer, A. J., Baordo, F., Bormann, N. and English, S. (2014). All-sky assimilation of microwave humidity sounders. *Technical Report 741*, ECMWF Tech. Memo., doi:10.21957/obosmx154, URL <https://www.ecmwf.int/node/9507>.

- Lawrence, H., Bormann, N., Geer, A. J., Lu, Q. and English, S. J. (2018). Evaluation and assimilation of the microwave sounder MWHS-2 onboard FY-3C in the ECMWF numerical weather prediction system. *IEEE T. Geosci. Remote Sens.*, **56**(6), 3333–3349, doi:10.1109/TGRS.2018.2798292.
- Lawrence, H., Bormann, N., Sandu, I., Day, J., Farnan, J. and Bauer, P. (2019). Use and impact of Arctic observations in the ECMWF numerical weather prediction system. *Quart. J. Roy. Meteor. Soc.*, **145**(725), 3432–3454, doi:10.1002/qj.3628, URL <https://rmets.onlinelibrary.wiley.com/doi/abs/10.1002/qj.3628>.
- Lean, P., Geer, A. and Lonitz, K. (2017). Assimilation of Global Precipitation Mission (GPM) Microwave Imager (GMI) in all-sky conditions. *Technical Report 799*, ECMWF Tech. Memo., doi:10.21957/8orc7sn33, URL <https://www.ecmwf.int/node/17174>.
- Lonitz, K. and Geer, A. J. (2020). Reducing the drying effect through a water vapour correction to the all-sky error model. *Technical Report 53*, EUMETSAT/ECMWF Fellowship Programme Research Report, doi:10.21957/qmy8utbgb, URL <https://www.ecmwf.int/node/19528>.
- Lu, Q., Lawrence, H., Bormann, N., English, S., Lean, K., Atkinson, N., Bell, W. and Carminati, F. (2015). An evaluation of FY-3C satellite data quality at ECMWF and the Met Office. *Technical Report 767*, ECMWF Tech. Memo., doi:10.21957/317g9nqun, URL <https://www.ecmwf.int/node/14692>.
- McNally, T., Bonavita, M. and Thépaut, J.-N. (2014). The role of satellite data in the forecasting of Hurricane Sandy. *Mon. Weather Rev.*, **142**(2), 634–646, doi:10.1175/MWR-D-13-00170.1.
- Njoku, E. G. (1982). Passive microwave remote sensing of the Earth from space—A review. *Proc. IEEE*, **70**(7), 728–750, doi:10.1109/PROC.1982.12380.
- Rodgers, C. D. (1976). Retrieval of atmospheric temperature and composition from remote measurements of thermal radiation. *Rev. Geophys.*, **14**(4), 609–624, doi:10.1029/RG014i004p00609.
- Weston, P. and Bormann, N. (2018). Enhancements to the assimilation of ATMS at ECMWF: Observation error update and addition of NOAA-20. *Technical Report 48*, EUMETSAT/ECMWF Fellowship Programme Research Report, URL <https://www.ecmwf.int/node/18744>.
- Weston, P., Geer, A. J. and Bormann, N. (2019). Investigations into the assimilation of AMSU-A in the presence of cloud and precipitation. *Technical Report 50*, EUMETSAT/ECMWF Fellowship Programme Research Report, doi:10.21957/ewahn9ce, URL <https://www.ecmwf.int/node/19221>.